Solar-driven absorption cycle for space heating and cooling

Manel Vallès*, Mahmoud Bourouis, Dieter Boer

Universitat Rovira i Virgili, Departament d'Enginyeria Mecànica, Av. Països Catalans 26, 43007 Tarragona, Spain
Correponding author: e-mail: manel.valles@urv.cat

ABSTRACT

The Energy Performance of Buildings Directive (EPBD) requires that all new buildings in the European Union be nearly zero energy buildings (NZEB) by the end of 2020. Consequently, energy saving measures must be introduced in the design phase. However, in most cases there will still be a cooling and heating demand, which could be satisfied using renewable energy. Of all of the renewable energy resources, solar energy has been given most attention since it is CO_2 neutral.

The present study investigates a new solar thermally-driven system that meets the heating and cooling demands of buildings. This system consists of a reversible absorption cycle, which operates as a single-effect absorption cycle in the cooling mode and as a heat transformer in the heating mode. The components of both cycles are the same, and only the flow direction inside the system changes.

The working pair selected was ammonia-lithium nitrate so no rectifier is required and there are no problems of refrigerant freezing at low condensing temperatures when the cycle operates as a heat transformer. For both cycles, a mathematical model is developed to obtain feasible driving temperatures and evaluate the cycle's coefficient of performance (COP) depending on the ambient temperature.

The results show that in the heating mode, the heat transformer cycle can be driven with a heat source at 40 °C to produce hot water at 55 °C at an ambient temperature of 0 °C and a COP of about 0.45. In addition, the lower the ambient temperature, the higher the hot water temperature that the heat transformer can produce. In the cooling mode, the single-effect absorption cycle can be driven with a heat source at 85 °C to produce chilled water at 7 °C at an ambient temperature of 30°C and a COP of 0.6. As a result, this configuration overcomes the limitations of existing absorption cycles and presents an interesting alternative to existing heating and cooling systems.

Keywords: solar heating and cooling; absorption cooling; absorption heat transformer; ammonia-lithium nitrate; reversible absorption cycle

1. Nomenclature

A	Absorber
C	Condenser
COP	Coefficient of performance
CR	Circulation ratio
CV	Closing valve
E	Evaporator
EV	Expansion valve
G	Generator
GTL	Gross temperature lift (°C)
h	Specific enthalpy (kJ/kg)
m	Mass flow rate (kg/s)
P	Pump
p	Pressure (kPa)
Q	Heat rate (kW)

SHE	Solution heat exchanger
SSAR	Single stage absorption refrigeration
SSAHT	Single stage absorption heat transformer
T	Temperature (°C)
W	Pump power consumption (kW)
w	Lithium nitrate mass fraction

Greek letters

ε	Effectiveness (%)
η	Efficiency (%)
ρ	Solution density (kg/m^3)

Subscripts

A	Absorber
C	Condenser
E	Evaporator
G	Generator
H	High
L	Low
P	Pump
PR	Refrigerant pump
PS	Solution pump
R	Refrigerant
S	Solution
SHE	Solution heat exchanger

1. Introduction

The increasing access to energy has improved the living conditions of people all around the world. Nevertheless, this continuous increase in the consumption of energy, which is mainly based on fossil fuels, has caused our society to face three fundamental problems: global warming, atmospheric pollution and a strong dependency on a finite supply of fossil fuels. The European Union has taken the fight against these problems very seriously and adopted several directives fostering the use of renewable energy sources and the maximum harnessing of energy to reduce the waste of resources as much as possible.

The Energy Performance of Buildings Directive (EPBD) requires that all new buildings in the European Union be nearly zero energy buildings (NZEB) by the end of 2020 [1]. As a result, energy efficiency measures must be considered in the design phase. However, in most cases there will still be a cooling and heating demand, and this has encouraged an interest in meeting heating and cooling demands with renewable energy.

Solar energy can contribute to meet the heating and cooling demands of buildings by solar electricity or solar thermally driven processes [2]. Electricity-driven reversible compression heat pumps connected to photovoltaic modules are an attractive solution as long as the local utility allows the connection to the grid. In isolated photovoltaic installations, the high cost and environmental impact of batteries may mean that the accumulation of electricity in batteries for operation is not viable outside sunny hours. So, heat storage for heating and cooling are needed to compensate for mismatches between the solar radiation available and the building loads [3]. Even so, at ambient temperatures below 0°C the maximum temperature of current electrical compression single-stage heat pumps is below 55 °C, too low for conventional heating systems [4].

In thermally-driven systems, solar thermal collectors convert solar energy into thermal heat, which can be used to run a thermally-activated device. Different types of thermally-driven cooling systems are available on the market and, of these, absorption systems are the most mature technology [5].

Solar absorption cooling has been actively investigated for nearly twenty years and has generated a wealth of theoretical and experimental literature, much of which has been collected in literature review papers [6-12]. The literature review in [6] concludes that the average normalized collector area and COP for the studies considered are 4.67 m^2/kW and 0.68, respectively. The average regeneration temperature used to drive the solar absorption cycle is 88.5 °C.

Solar absorption heating has been studied much less than solar absorption cooling. The thermal collectors mostly used by solar absorption cooling installations are flat plate or evacuated tubes.

However, these solar collectors provide a hot water temperature in winter that is is too low to drive commercial absorption cycles when they have to operate as heat pumps for heating in winter. Wu et al. [12] modeled the performance of various air-source absorption heat pumps using NH_3-H_2O. They compared the performance of a single-effect absorption heat pump and a GAX cycle with direct solar heating. They concluded that with a flat collector, the system efficiency of the absorption heat pump is far lower than the solar efficiency of the direct solar heating system. Although the absorption cycle achieves a COP of 1.3-1.5, the high activation temperatures required by the cycle, reduce the collector efficiency to below 0.3. Seeing the limitations imposed by the high activation temperatures of the cycle, other authors [13,14] have proposed activating the absorption heat pump with a boiler and using the solar energy of the collectors in the evaporator to save more energy than a conventional system with a boiler. Along these lines, Wu et al [13] modeled an air-source absorption heat pump using NH_3-H_2O, NH_3-$LiNO_3$ and NH_3-NaSCN as working fluids. The results indicate that NH_3-$LiNO_3$ requires a lower generating temperature, and can work at a lower evaporating temperature and a higher condensing temperature.

On the other hand, the temperature of the hot water produced in the solar collectors is too low on cold days to directly feed conventional heating systems with radiators. A similar situation takes place at the end of the winter season in district heating systems integrated with solar energy and a seasonal thermal energy storage. In both cases, an alternative would be to operate the absorption cycle as an absorption heat transformer, which can upgrade up to 50% of the heat supplied at low temperature to more useful levels [15-16].

To date, absorption heat transformers have mainly been installed in distillation plants, the pulp and paper industry and synthetic rubber factories [16]. Most published works are theoretical simulation studies, small-scale applications for water purification or steam production prototypes [16]. In all industrial applications and in the majority of theoretical studies or pilot plants, the working fluid mixtures used are the traditional ones (namely H_2O-LiBr and NH_3-H_2O). But these conventional working pairs have certain limitations when the absorption heat transformer is integrated into a heating system in winter. For instance, the H_2O-LiBr mixture cannot be used with negative ambient temperatures because water freezes at 0°C. The NH_3-H_2O mixture does not have this problem but requires rectification that adds complexity to the cycle and reduces the COP.

Due to these limitations, this study proposes the mixture NH_3-$LiNO_3$ as the working fluid for a reversible absorption cycle. In heating mode, the absorption cycle would operate as a heat transformer to upgrade low-temperature heat sources. In cooling mode, it would operate as a single-effect absorption chiller.

The NH_3-$LiNO_3$ mixture has already been proposed in two previous studies for use in heat transformers [17-18]. However, these studies focus on higher heat source and environment temperatures.

This mixture has also been proposed in many investigations for use in absorption refrigeration systems and some of these studies [21-23] compare the performance of this mixture with other working mixtures in absorption cooling systems. Theoretical investigations report that the NH_3-$LiNO_3$ absorption cycle can operate at lower temperature of the driving heat and high COP than the NH_3-H_2O absorption cycle. This perspective of the theoretical studies has also been confirmed in experimental prototype studies [24-26].

Although several studies have suggested that the NH_3-$LiNO_3$ mixture can be used in solar cooling absorption systems, to our knowledge, none have proposed coupling an absorption heat transformer with this mixture to a solar panel to upgrade the temperature of solar heat. Moreover, the main novelty of the present study lies in the operational modes of the system proposed, which could operate either as an absorption chiller or as an absorption heat transformer.

Therefore, this study proposes a new solar thermally-driven system that meets the heating and cooling demands of buildings. The system consists of a reversible absorption unit, which operates as a single-stage absorption cycle for cooling and as an absorption heat transformer for heating. The components of both cycles are the same; however, the internal flow direction and the operating conditions of the components change.

2. Description of the system

Fig. 1 illustrates the main components of a single-stage absorption refrigeration (SSAR) cycle and a single-stage heat transformer (SSAHT) cycle represented in a Pressure-Temperature plot. As can be seen, both cycles consist of the same five heat exchangers: an absorber, a generator, a condenser, an evaporator and a solution heat exchanger. The only difference is that the heat transformer cycle includes two pumps – one in the solution circuit and another in the refrigerant circuit – and only one expansion valve in the solution circuit, while the absorption refrigeration cycle has only one solution pump in the solution circuit and two expansion valves in the solution and refrigerant circuits.

Both cycles operate at two pressure levels. In the case of SSAR, the condenser and generator are on the high-pressure side while the absorber and the evaporator are on the low-pressure side. For SSAHT, it is the opposite. Both cycles operate at three temperature levels. The difference is that in the SSAHT driving heat (Q_E) is supplied at an intermediate level (T_E=T_G) to evaporate the refrigerant in the evaporator and to boil the solution in the generator (Q_G). On the other hand, the cycle produces heat at a higher temperature (T_A) in the absorber (Q_A) and dissipates heat at a lower temperature (T_C) in the condenser (Q_C) in the process of absorption and condensation of the refrigerant, respectively. In the case of the SSAR, driving heat is supplied at a high temperature (T_G) in the generator, which produces the cooling effect at a low temperature in the evaporator (T_E) while heat is dissipated at an intermediate temperature in the absorber (T_A) and condenser (T_C).

To sum up, a SSAHT could be said to be a SSAR operating inversely. Also, the objective of both cycles is different: SSAHT can recover heat available at a medium temperature (T_E=T_G), upgrade it to useful heat at a higher temperature (T_A), and reject some heat at ambient temperature (T_C); while SSAR

produces cooling at low temperature (T_E), and rejects heat at ambient temperature (T_C=T_A) thanks to the driving heat supplied at high temperature (T_G).

Fig. 2 shows a schematic diagram of the machine that can operate as a SSAR for cooling and as a SSAR for heating. The continuous line and dashed line represent the circulation of the solution and refrigerant streams for the SSAR and the SSAHT, respectively. The first letter of each component indicates the function of the heat exchanger when it operates as a SSAR. As far as the solution circuit is concerned, although the position of the absorber and generator is reversed, the circuit does not change. Although the diagram shows two circuits to clarify the circulation of each cycle in the machine, actually there is only one. On the other hand, refrigeration side requires two circuits because the SSAR needs an expansion valve but the SSAHT needs a refrigerant pump. Automatic shut-off valves isolate the non-operational circuit.

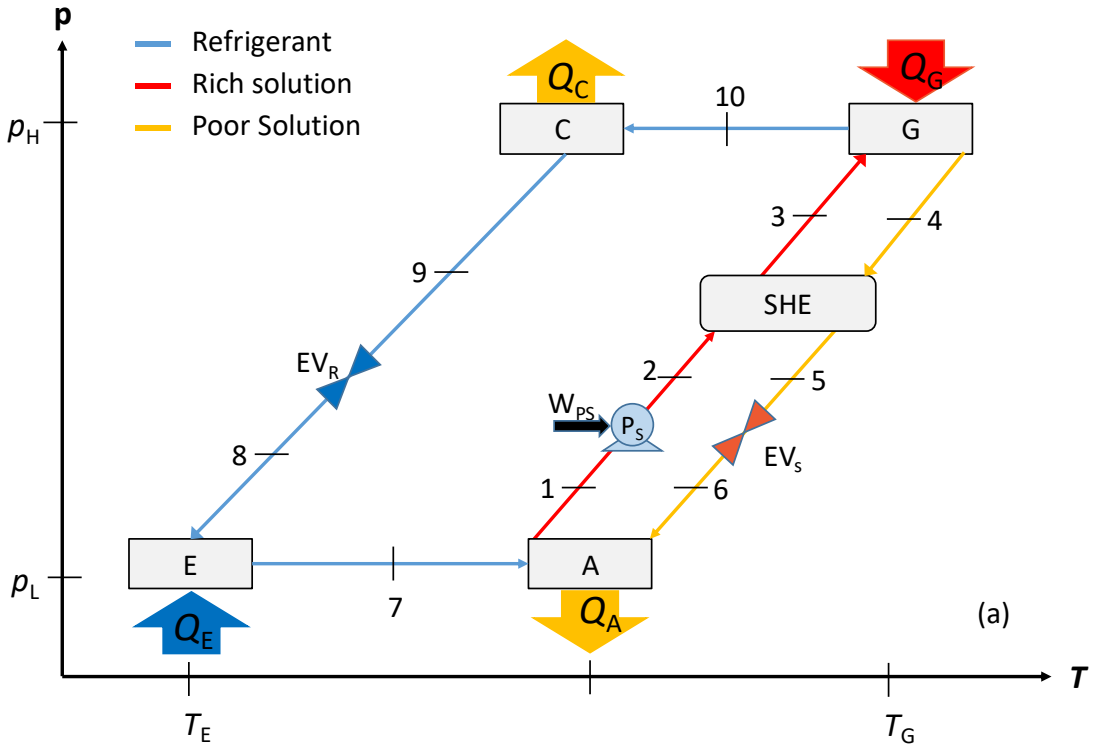

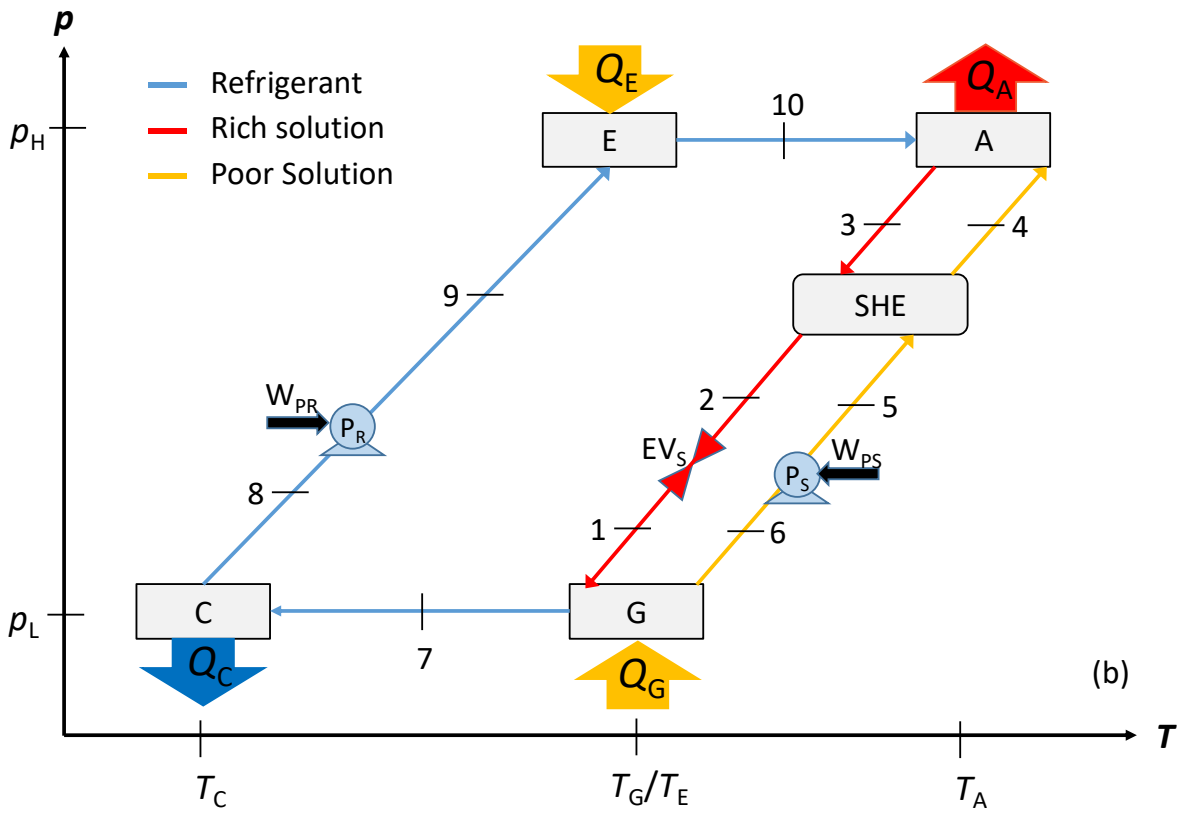

Figure 1. P-T diagram for a SSAR (a) and a SSAHT (b)

Plate heat exchangers could be used in all thermal components of the system, using glycol solutions or water, as external thermal fluids, to provide or dissipate heat in each component. In order to dissipate to the environment, the heat released in the absorber and the condenser of SSAR or the condenser of SSAHT, the use of a dry cooler is proposed. In a building, it results difficult to justify the use of a wet cooling tower for maintenance costs and hygienic-health risks. In addition, the wet cooling tower could not be used to dissipate the heat of SSAHT condenser if the ambient temperature is below 0 °C.

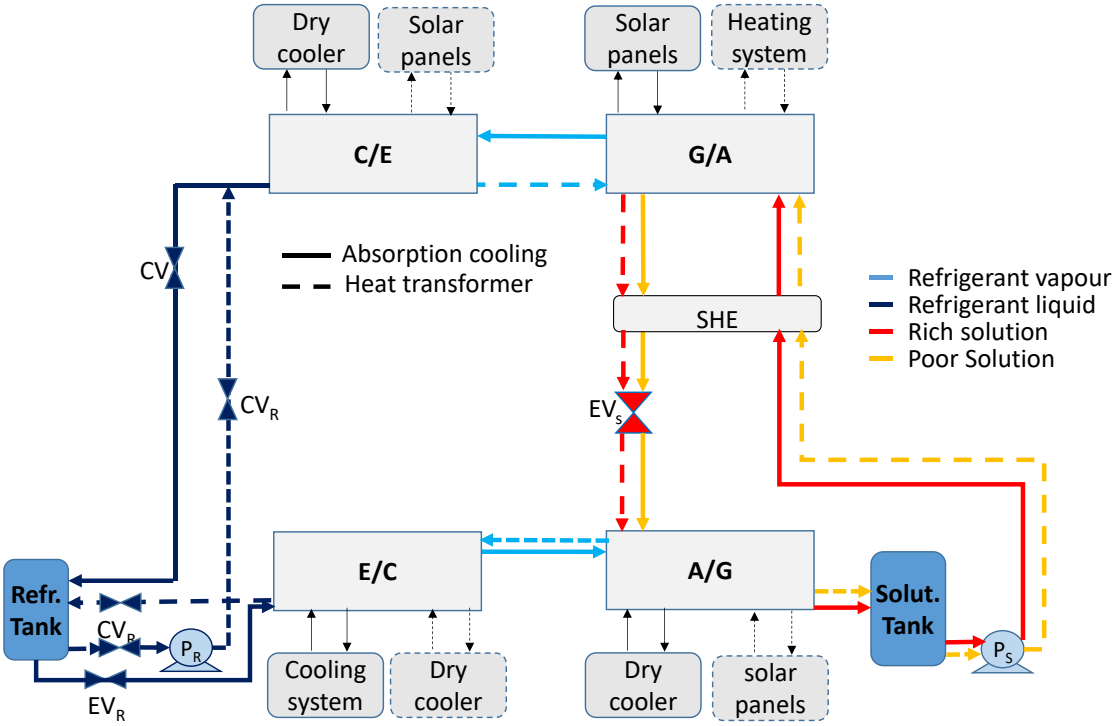

Figure 2. Schematic diagram of the system

An analysis of the literature enables us to draw the following conclusions about the reversibility of the cycle and the mixture NH_3-$LiNO_3$ as working pair. Because of the low heat and mass transfer coefficients, the absorber is the biggest component in absorption systems, and its performance directly impacts the overall size and energy performance of these devices [27]. However, the experimental data on the absorption and desorption processes of the NH_3-$LiNO_3$ mixture in plate exchangers indicate that the heat and mass transfer coefficients are quite similar in both cases. For instance, Oronel et al. [28] presented an experimental study of bubble absorption in a plate heat exchanger using NH_3-$LiNO_3$. Experiments were carried out at a nominal system pressure of 510 kPa using a corrugated plate heat exchanger formed by three channels in which absorption takes place in the central one. The results indicate that, for a solution mass flux around 50 kg/s.m^2, the heat transfer coefficient ranges from 3 to 5 kW/m^2.K and the mass transfer coefficient from 0.9 to 1.2 m/h. On the other hand, Táboas et al. [29] experimentally determined the flow boiling heat transfer coefficient of NH_3-$LiNO_3$ using the same plate heat exchanger. The results indicate that, for the same solution mass flux, the boiling heat transfer coefficient is between 2.5 and 3.5 kW/m^2.K. Therefore, the heat transfer coefficient in the absorber is even higher and the pair of heat exchangers that exchange their role between absorber and generator must be designed according to the maximum generation heat of the two cycles. As regards the evaporator/condenser pair, the heat transfer coefficients of ammonia condensation in plate exchangers are up to twice as high as those of evaporation [30]. Therefore, the sizing of these two components must be based on evaporation heat transfer coefficients in plate exchangers that are between 6 and 7 kW/m^2 K for evaporation temperatures higher than -10 °C [30, 31].

3. Modeling assumptions

The following assumptions have been made for the thermodynamic simulation of both cycles:

- Operating conditions are steady state.
- Frictional pressure losses in the heat exchangers and pipes and gravitational pressure drops are negligible.
- At the exit of the condenser and evaporator, the refrigerant is saturated.
- The solution is at equilibrium at the exit of generator and absorber.

- Expansion in the valves is assumed to be isenthalpic.
- Heat losses to the surrounding in the components and pipes of the cycle are negligible.
- The pump efficiency is set at a constant value η_P= 50%.
- The effectiveness of the solution heat exchanger is set at a value of ε_{SHE}=85%, unless otherwise stated.
- The solution pump delivers a constant flow rate of 1 kg/s.

4. Governing equations and properties of the working pair

In order to analyze the feasibility and performance of the system to produce chilled water in summer and hot water in winter from a heat source supplied by solar thermal panels, a simulation tool was developed in the Engineering Equation Solver (EES) environment. The system performance is expressed as the coefficient of performance (COP).

The mathematical model is based on the global mass, species and energy balance equations in each component of the cycle. If the kinetic and potential energies are neglected, these equations in steady-state processes with reference to Figure 1 are as follows:

Table 1. Mass, species and energy balance equations in the components of the system

	SSAR	SSAHT
Evaporator (E)	$Q_E = m_7 h_7 - m_8 h_8$ *(1)*	$Q_E = m_{10} h_{10} - m_9 h_9$ *(15)*
Condenser (A)	$Q_C = m_9 h_9 - m_{10} h_{10}$ *(2)*	$Q_C = m_8 h_8 - m_7 h_7$ *(16)*
Absorber (A)	$m_6 + m_7 = m_1$ *(3)*	$m_4 + m_{10} = m_3$ *(17)*
	$m_6(1 - w_6) + m_7 = m_1(1 - w_1)$ *(4)*	$m_4(1 - w_4) + m_{10} = m_3(1 - w_3)$ *(18)*
	$Q_A = m_1 h_1 - m_6 h_6 - m_7 h_7$ *(5)*	$Q_A = m_3 h_3 - m_4 h_4 - m_{10} h_{10}$ *(19)*
Generator (G)	$m_3 = m_4 + m_{10}$ *(6)*	$m_1 = m_6 + m_7$ *(20)*
	$m_3(1 - w_3) = m_4(1 - w_4) + m_{10}$ *(7)*	$m_1(1 - w_1) = m_6(1 - w_6) + m_7$ *(21)*
	$Q_G = m_4 h_4 + m_{10} h_{10} - m_3 h_3$ *(8)*	$Q_G = m_6 h_6 + m_7 h_7 - m_1 h_1$ *(22)*
Solution Pump (P_S)	$\eta_P = \frac{1}{\rho_1}\frac{p_{high} - p_{low}}{h_2 - h_1}$ *(9)*	$\eta_P = \frac{1}{\rho_6}\frac{p_{high} - p_{low}}{h_5 - h_6}$ *(23)*
	$W_{PS} = m_2 h_2 - m_1 h_1$ *(10)*	$W_{PS} = m_5 h_5 - m_6 h_6$ *(24)*
Refrigerant Pump (P_R)		$\eta_P = \frac{1}{\rho_8}\frac{p_{high} - p_{low}}{h_9 - h_8}$ *(25)*
		$W_{PR} = m_9 h_9 - m_8 h_8$ *(26)*
Solution Heat exchanger (SHE)	$m_2(h_2 - h_3) + m_4(h_4 - h_5) = 0$ *(11)*	
	$\epsilon_{SHE} = \frac{m_4(h_4 - h_5)}{min\left(m_4(h_4 - h_{5(T_5 = T_2)}); m_2(h_{3(T_3 = T_4)} - h_2)\right)}$ *(12*	$\epsilon_{SHE} = \frac{m_4(h_4 - h_5)}{min\left(m_4(h_{4(T_4 = T_3)} - h_5); m_2(h_3 - h_{2(T_2 = T_5)})\right)}$ *(27)*
COP	$COP = \frac{Q_E}{(Q_G + W_{PS})}$ *(13)*	$COP = \frac{-Q_A}{(Q_G + Q_E + W_{PS} + W_{PR})}$ *(28)*
CR	$CR = \frac{m_2}{m_7}$ *(14)*	$CR = \frac{m_5}{m_7}$ *(29)*
GTL		$GTL = T_A - T_E$ *(30)*

In order to solve the mass and energy balances of the mathematical model, the thermophysical properties of working fluids are required. The thermodynamic and transport properties of ammonia are obtained from the equation of Tillner-Roth [32] implemented in the EES. Meanwhile, for the NH_3-$LiNO_3$ mixture, the following equations obtained from Salavera and Coronas [33], valid from 0.2 to 0.65 in ammonia mass fraction and up to 150 ºC, are used.

$$ln(p) = (a_o + a_1 w) + \frac{1}{T}\sum_{i=0}^{4} b_i\, w^i + c_0 \cdot ln(T + 273.15) + d_0 \cdot (T + 273.15) \quad (34)$$

$$h = \sum_{i=0}^{4} c_i w^i + (a_0 + a_1 w)T + 0.5(b_0 + b_1 w)[T(T + 2 * 273.15)] \quad (35)$$

$$\rho = \frac{a_o + a_1 w + a_2 w^2}{(b_o + b_1 w + b_2 w^2)\left[1 + \left(1 - \frac{T + 273.15}{c_0 + c_1 w}\right)^{d_0}\right]} \quad (36)$$

In these equations, p is the vapor pressure in kPa, ρ is the density in kg/m^3, h is the specific enthalpy in kJ/kg, w is the lithium nitrate mass fraction and T is the temperature in °C. The value of the regression coefficients for Eq. 34-36 are given in Table 2.

Table 2. Coefficients of Eq. 34-36 for the thermophysical properties of the NH_3-$LiNO_3$ solution

Coefficient	**Pressure**	**Enthalpy**	**Density**
a_0	83.57524472	2.1662	60.257249
a_1	0.603133	-2.0375	376.38
a_2	-	-	568.11
a_3	-	-	-
b_0	-4669.7	0.008866	0.25443
b_1	-257.676	-0.005756	0.7712
b_2	-834.214	-	-0.28135
b_3	1883.30	-	-
b_4	-5422.44	-	-
c_0	-11.607	200.00	405.65
c_1	-	-768.23	0.1086
c_2	-	-615.94	-
c_3	-	2266.1	-
c_4	-	-837.17	-
d_0	0.01719	-	0.288

5. Results

A parametric study was carried out to analyze the feasibility and limitations of the system to provide air conditioning throughout the year from solar thermal energy. Then, the coefficient of performance (COP) and the cooling capacity Q_E for SSAR and the COP and heating capacity Q_A for SSAHT were plotted versus the main operation parameters. The results reported here are all obtained with a solution pump flow rate of 1 kg/s. Table 3 shows the thermodynamic properties at various state points and the energy flows to and from each component of both cycles in the reference conditions shown in Table 4.

Table 3. Thermodynamic parameters at various state points of the SSAR and SSAHT cycles

State point	SSAR					SSAHT				
	T	p	w	m	h	T	p	w	m	h
1	40.0	517	0.50	1.00	9.3	18.3	430	0.40	1.32	82.5
2	40.7	1555	0.50	1.00	11.4	49.4	1555	0.40	1.32	82.5
3	76.0	1555	0.50	1.00	122.0	60.0	1555	0.40	1.32	119.6
4	85.0	1555	0.52	0.95	141.7	57.1	1555	0.52	1.00	55.0
5	47.4	1555	0.52	0.95	25.6	40.7	1555	0.52	1.00	6.1
6	44.8	517	0.52	0.95	25.6	40.0	430	0.52	1.00	3.9
7	5.0	517	0.00	0.05	1467.3	40.0	430	0.00	0.32	1561.7
8	5.0	517	0.00	0.05	390.6	0.0	430	0.00	0.32	199.9
9	40.0	1555	0.00	0.05	390.6	0.6	1555	0.00	0.32	203.4
10	85.0	1555	0.00	0.05	1625.2	40.0	1555	0.00	0.32	1489.9
COP	0.57					0.46				
CR	21.0					3.2				
Q_E	51.1					406.2				
Q_C	58.6					430.0				
Q_G	90.1					388.5				
Q_A	84.8					368.0				
W_{PS}	2.0					2.16				
W_{PR}	-					1.1				

Units: T (°C), P (kPa), w (%), h (kJ/kg), Q (kW), W(kW).

Table 4. Nominal operating conditions for the cycle simulations

SSAR	SSAHT
T_E = 5 °C	T_C = 0 °C
$T_A = T_C$ = 40 °C	$T_G = T_E$ = 40 °C
T_G = 85 °C	T_A = 60 °C

5.1 Single-stage absorption refrigeration cycle (SSAR)

Figs. 3(a) and 3(b) show the COP values versus the generator temperature at an evaporation temperature of 5 and 10 °C, respectively. The evaporation temperature of 5 °C is the typical evaporation temperature for air conditioning systems with fan-coils while the temperature of 10 °C is that of an underfloor cooling system. Each figure shows the COP values at four absorber-condenser temperatures. The COP values for an absorption-condensation temperature of 30 °C could be for a geothermal dissipation system. In contrast, the other three absorption-condensation temperatures could occur for a dry-cooler with ambient temperatures between 30 and 40 °C. As can be seen, the COP remains almost constant and drops drastically when the generation temperature decreases because of the decrease in the concentration difference between the strong and weak solutions. Therefore, there is a lower limit of the generator temperature for each absorber-condenser temperature. By comparing the two figures, it can be observed that the higher the evaporation temperature and the lower the absorption-condensation temperature, the lower the low generator temperature limit. Approximately, a decrease of 5 °C in the evaporation temperature leads to an increase of 5 °C in the minimum generation temperature. Finally, it should be

noted that, even though the cycle can operate with very high dissipation temperatures, a geothermal dissipation system can provide COP values above 0.6 with very low solar collector temperatures. For instance, if a pinch temperature value of 5 °C is chosen in every heat transfer operation, the SSAR cycle can be driven with a heat source temperature of 85 °C to produce chilled water at 7 °C at a cooling water temperature of 30 °C with a COP of 0.6.

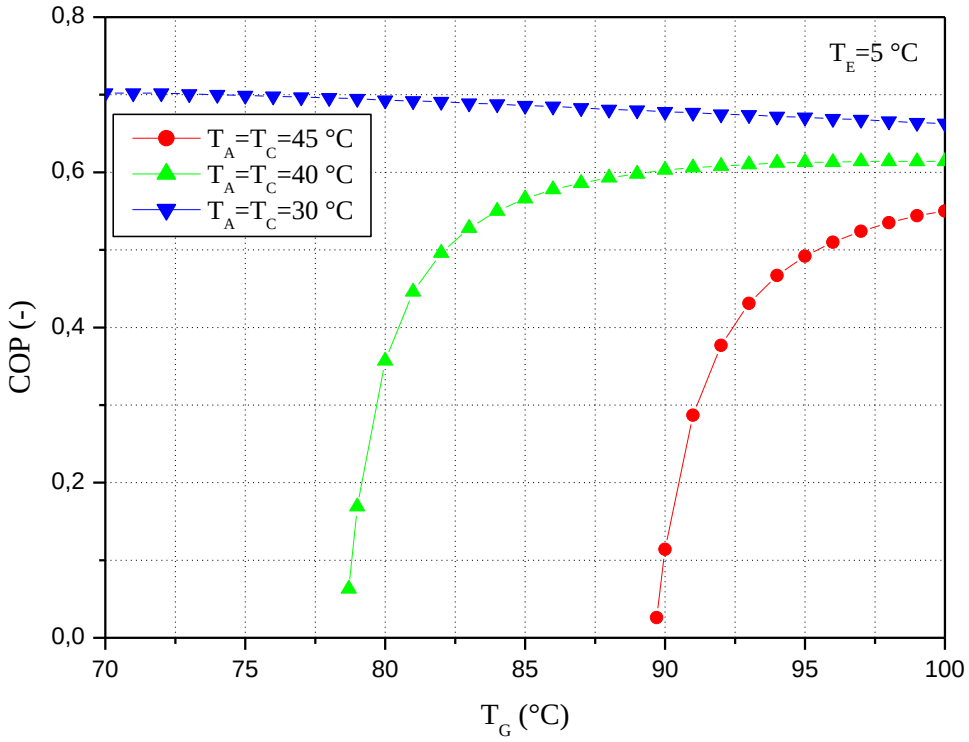

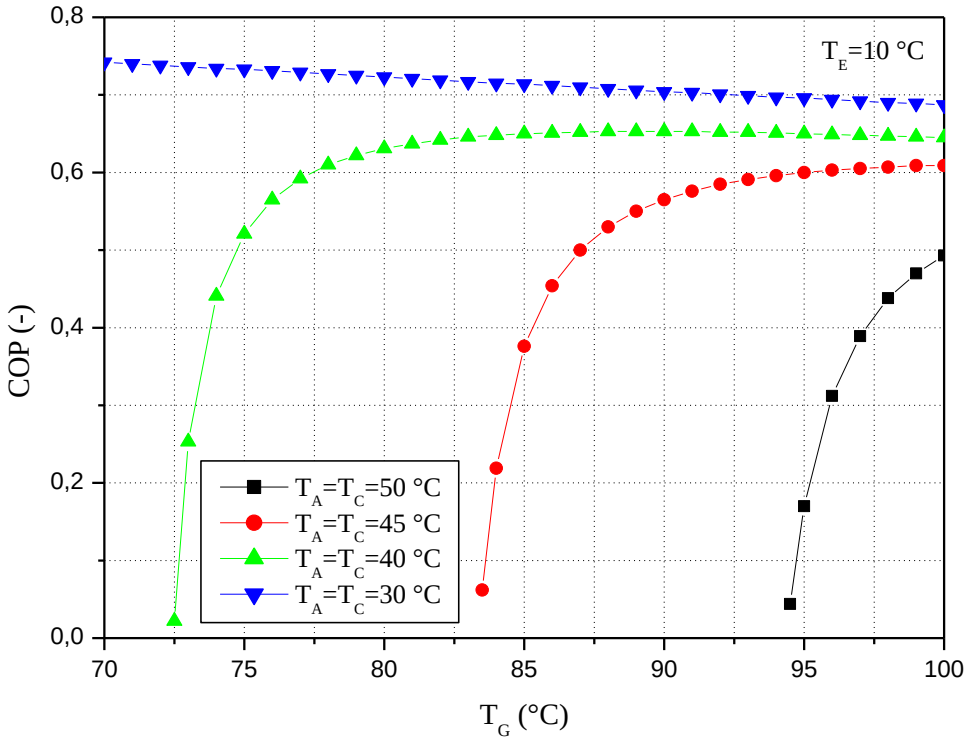

Figure 3. Effect of generator temperature on COP for SSAR at: (a) T_E= 5 °C; (b) T_E= 10 °C

Figures 4(a) and 4(b) show cooling capacity versus the generation temperature. It can be seen that in all cases, there is a significant reduction in the cooling capacity as the temperature of the generator decreases. As long as it does not approach the lower limit of the generator temperature, the temperature decrease of the hot water driving the generator allows the machine to operate at partial load without a COP penalty. In addition, it is worth noting the strong effect of the absorber-condenser temperature on the cooling capacity of the equipment. For instance, for a fixed generator temperature of 85 °C, the cooling capacity decreases from 231.9 to 51.1 kW when the temperature of the absorber-condenser increases by 10 °C from 30 to 40 °C at an evaporation temperature of 5 °C, and from 307.1.6 to 107.5 at an evaporation temperature of 10 °C.

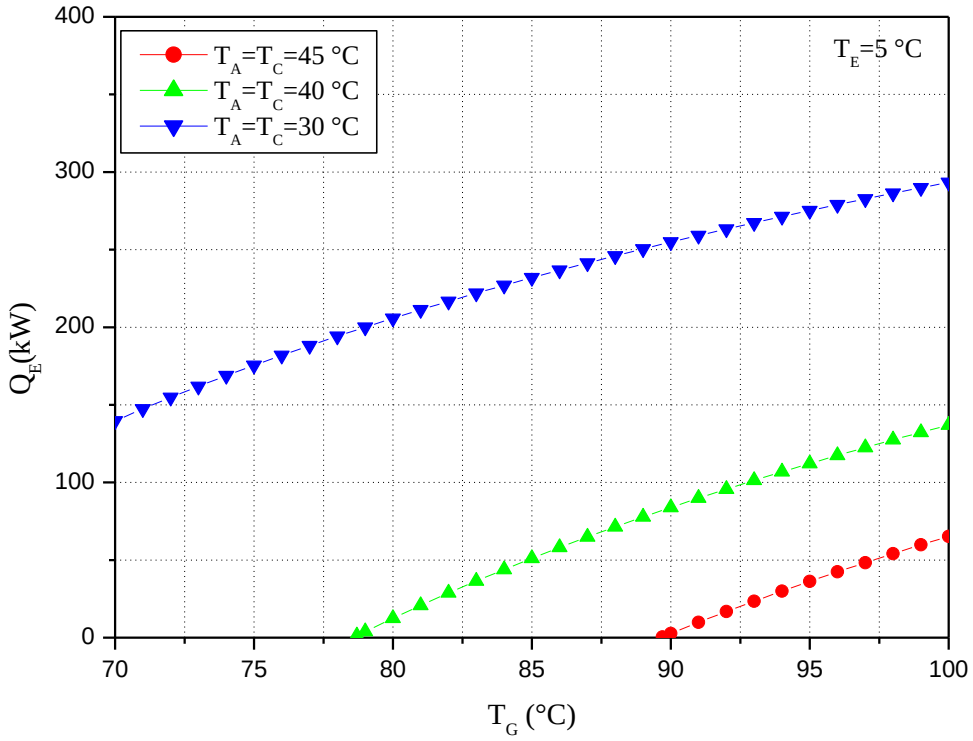

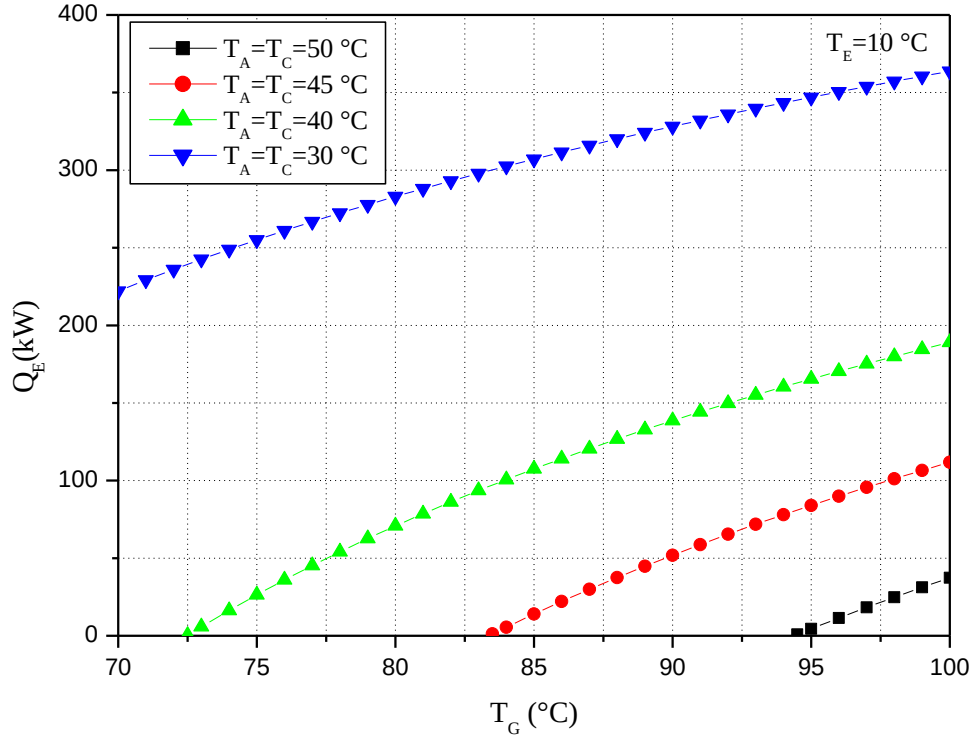

Figure 4. Effect of generator temperature on cooling capacity for SSAR at: (a) T_E= 5 °C; (b) T_E= 10 °C

Figures 5(a) and 5(b) show the corresponding comparison of circulation ratios (CR) versus generator temperature. The figures show that the circulation ratio achieves values below 10 when the flat COP zone is reached. When the generator temperature approaches its lower limit the circulation ratio

increases dramatically. Therefore, if the solution flow is kept constant, there will be a reduction in the cooling capacity, as seen in Figure 4.

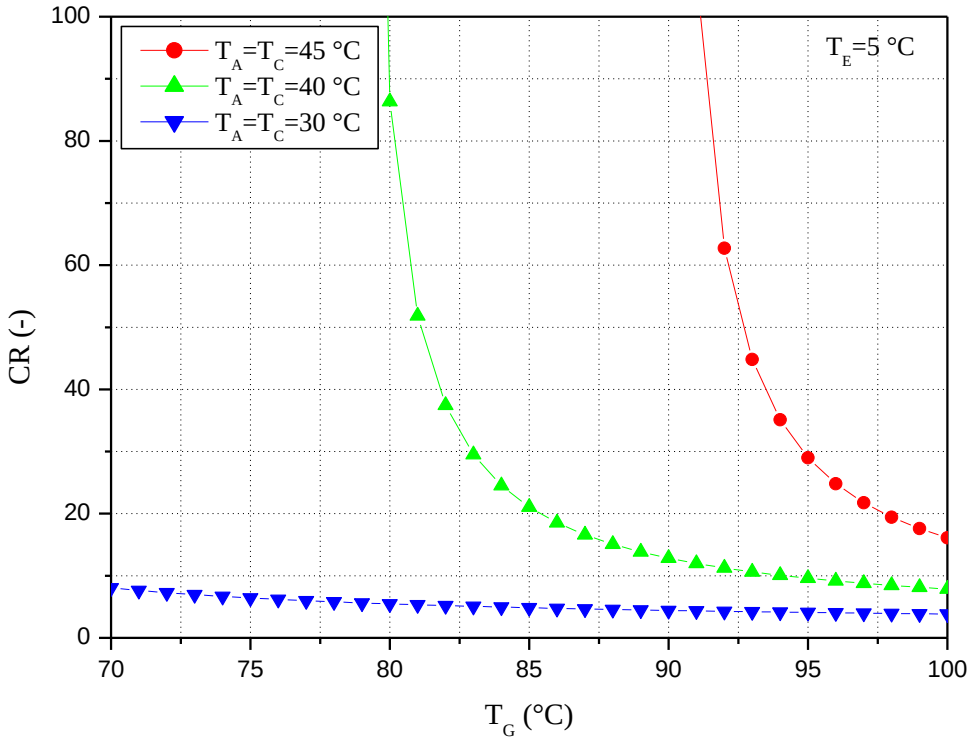

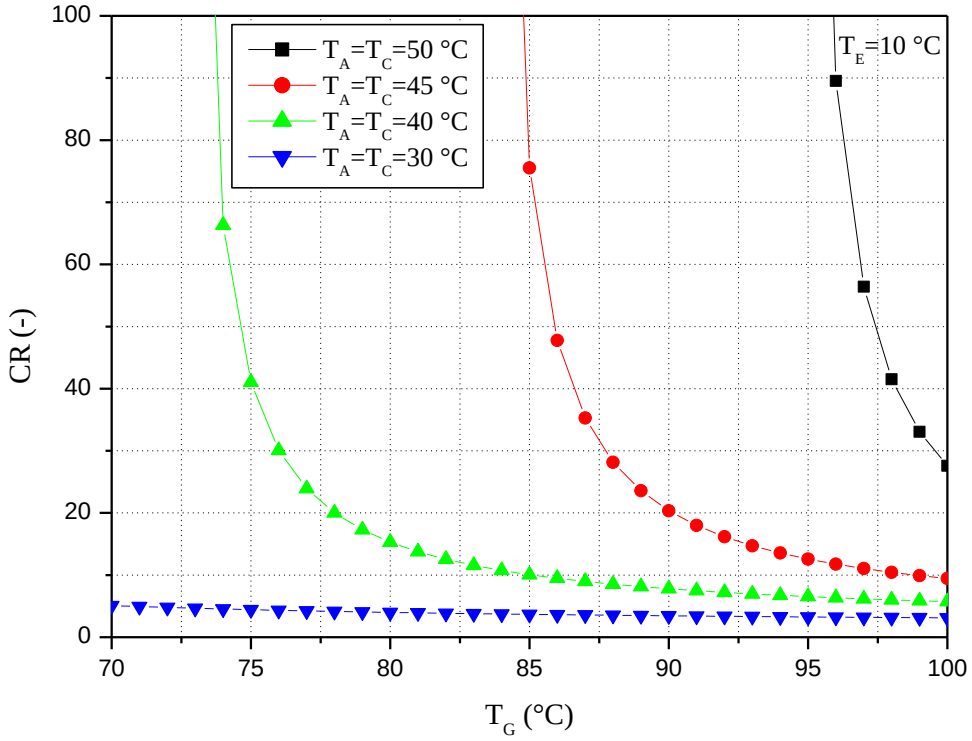

Figure 5. Effect of generator temperature on circulation ratio for SSAR at: (a) T_E= 5 °C; (b) T_E= 10 °C

To study the influence of solution heat exchanger effectiveness on performance, the COP of the SSAR at different generation temperatures is simulated at three different values of heat exchanger effectiveness. The absorption-condensing temperature considered is 35 °C and the evaporation

temperature 5°C. The results presented in Figure 6 indicate that the heat exchanger effectiveness has a reduced effect on the minimum activation temperature, although it has a significant effect on the COP. For instance, the COP decreases from 0.61 to 0.47 when the heat exchanger effectiveness is reduced from 0.9 to 0.7 at a fixed generation temperature of 85 °C.

The COP values, between 0.6 and 0.7 over a wide range, match the results presented in previous SSAR simulation studies with this mixture for air-conditioning purposes [34-36]. Also, CR values below 10 in the stable COP range, coincide with the literature results [35].

Although the literature results indicate that the H_2O-LiBr mixture gives higher COP values for these operating conditions [21], the freezing temperature of water means that it cannot even be considered for use in an air conditioning system that must operate all year round.

On the other hand, the literature results agree that with the proposed mixture, NH_3-$LiNO_3$, the cycle can operate at lower generator temperatures and with higher COP values than the traditional mixture NH_3-H_2O [19, 20, 23].

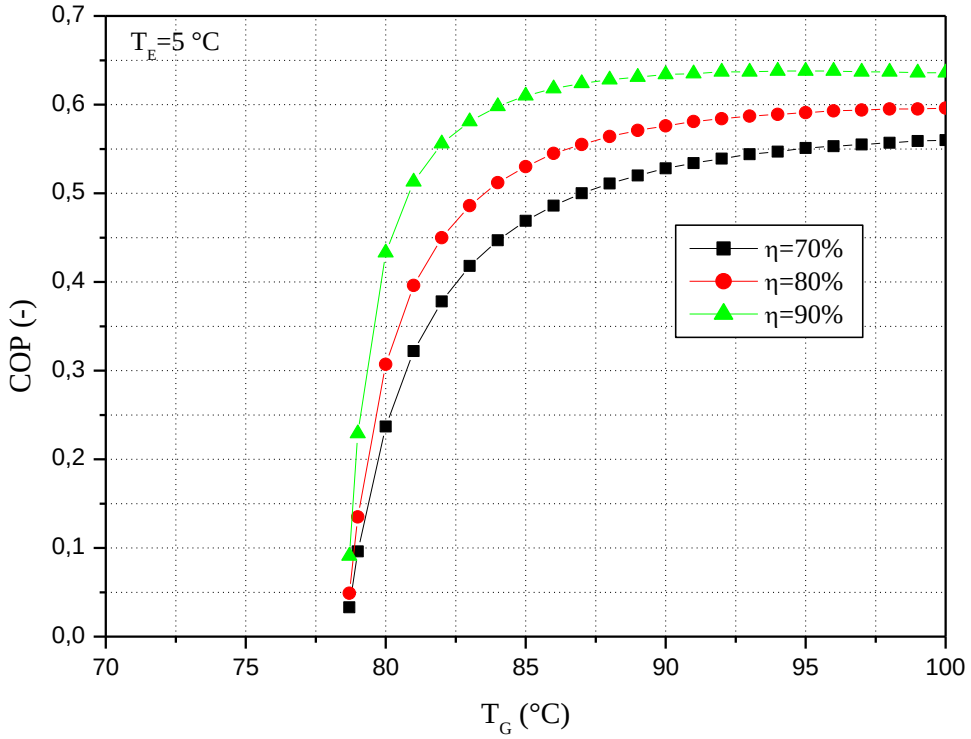

Figure 6. Effect of solution heat exchanger effectiveness on SSAR at T_E= 5 °C

5.2 Single-stage absorption heat transformer cycle (SSAHR)

Figures 7(a) and 7(b) show the COP values versus generator-evaporator temperatures at an absorption temperature of 60 and 50 °C, respectively. In this case, the absorption temperature of 60 °C is the typical absorption temperature for a conventional heating system with radiators, whereas the temperature of 50 °C is that of an underfloor heating system. As can be observed, the COP remains almost constant at a value close to 0.45 and drops drastically when the generation-evaporation temperature is decreased because of the smaller concentration difference between the strong and weak solutions. The condensation temperature, directly related to the ambient air temperature, marks the minimum temperature required for the cycle operation. For instance, at an absorption temperature of 50 °C and a condensation temperature of 0 °C, the cycle reaches a COP value of 0.45 at a generation-evaporation temperature of 27 °C, while at a condensing temperature of 10 °C a generation-evaporation temperature

of 32 °C is required. However, once the COP's stable zone is reached, there is no significant effect of the condensation temperature on the cycle COP. Moreover, it is worthy of note that, unlike the refrigeration cycle, the worse the environmental conditions are (low temperature in winter) the lower the activation temperatures the cycle can operate with.

If the pinch temperature is again considered to be 5 °C in every heat transfer operation, the SSAHT cycle can be driven with a heat source temperature of 40 °C to produce hot water at 55 °C at an ambient temperature of 0 °C and a COP close to 0.45.

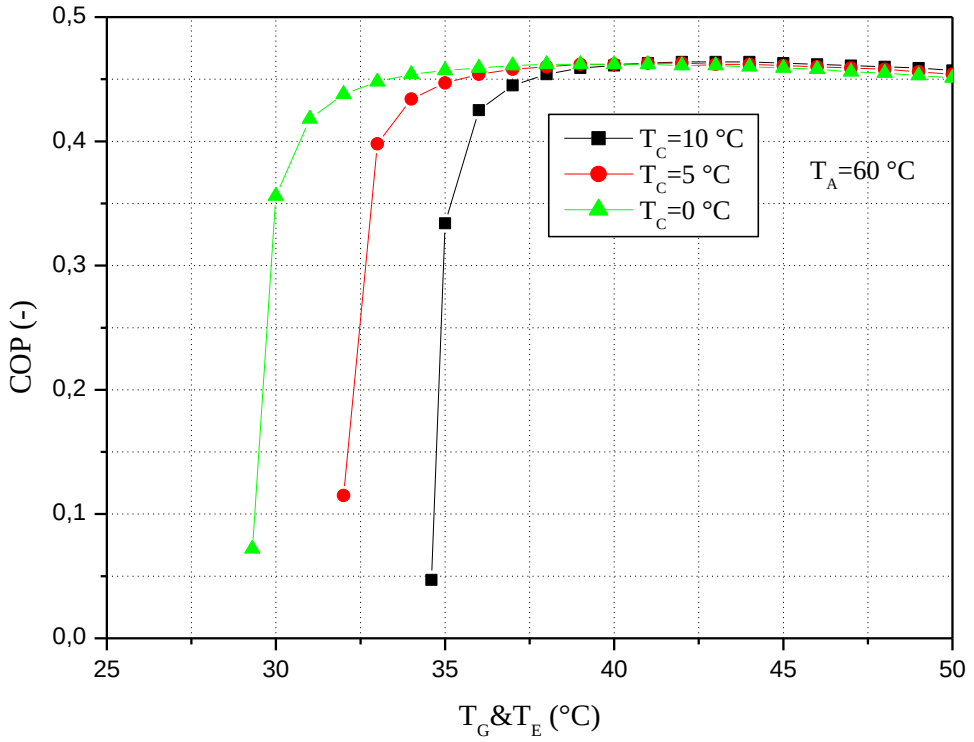

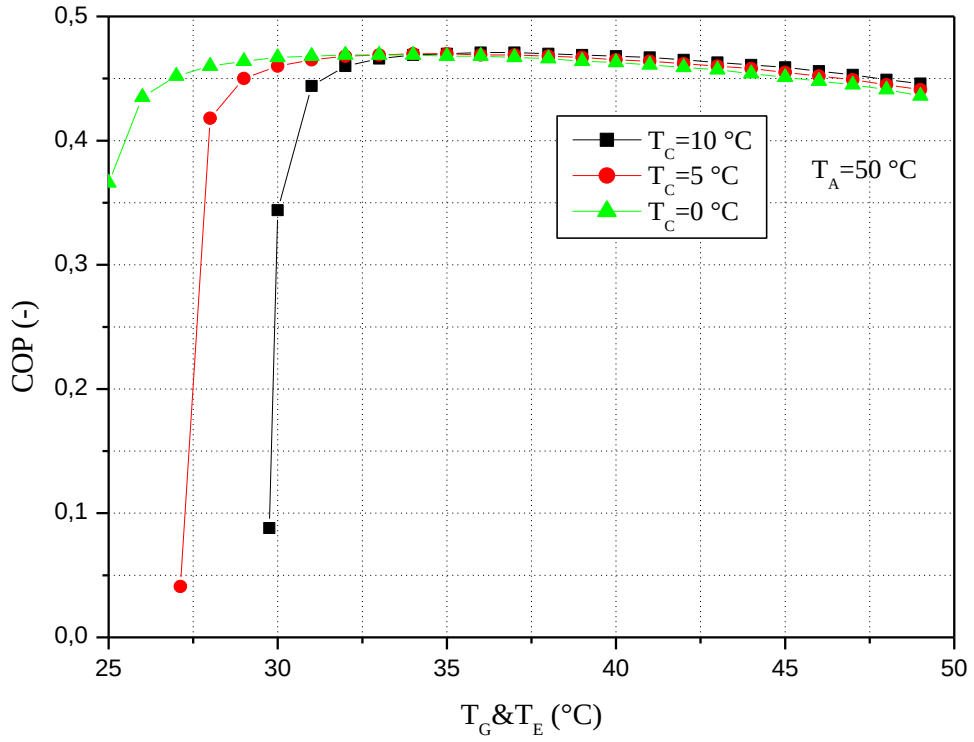

Figure 7. Effect of generator and evaporator temperature on COP for SSAHT at: (a) T_A= 60 °C; (b) T_A= 50 °C

Figures 8(a) and 8(b) show the effect of generation-evaporation temperatures on the heating capacity. It should be noted in this case that, contrary to what happens in the refrigeration cycle, when the climatic conditions get worse (that is to say, when the ambient temperature drops), the heating power of the equipment increases. For instance, at an absorber temperature of 60 °C and a generator-evaporator

temperature of 40 °C, the heating power increases from 206.7 to 367.8 kW when the condensing temperature drops from 10 to 0 °C. Also note that for most of the operating conditions presented, the power of the heating cycle is higher than that of cooling. This is because, for the selected operating conditions, the concentration difference between the strong and weak solutions is higher in the SSAHT cycle (see Table 3). Therefore, if the heating loads of the building are much higher than the cooling loads, these could be achieved as long as the heat exchangers are sized for these capacities. Moreover, the almost linear variation of the machine power with the temperature of the driving heat indicates that a simple control can be used for the machine functioning at partial load.

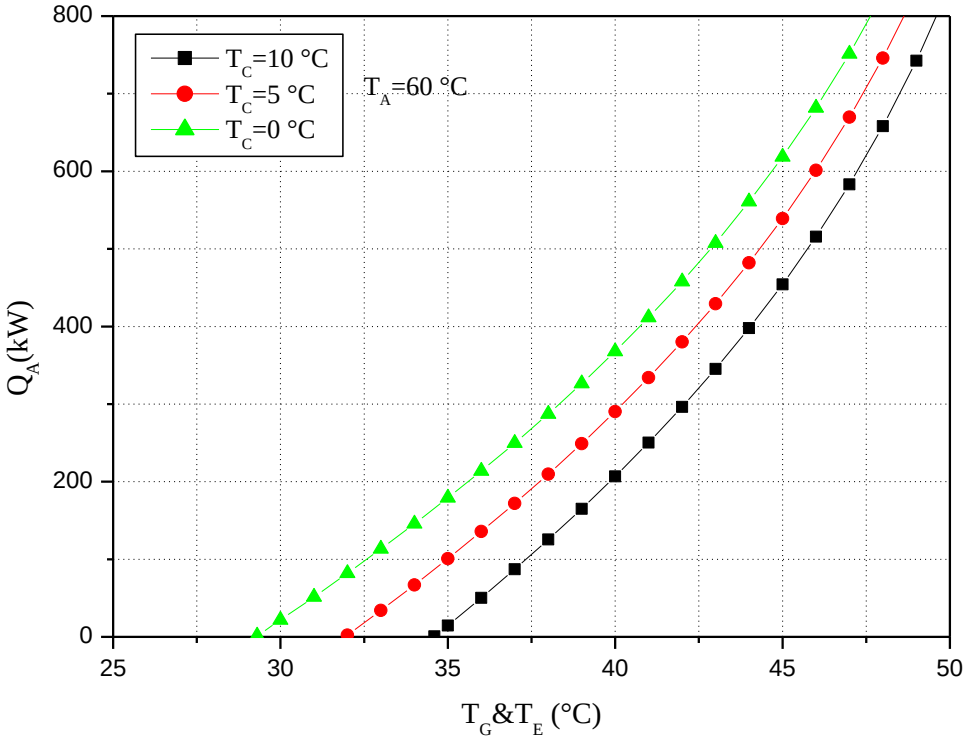

406

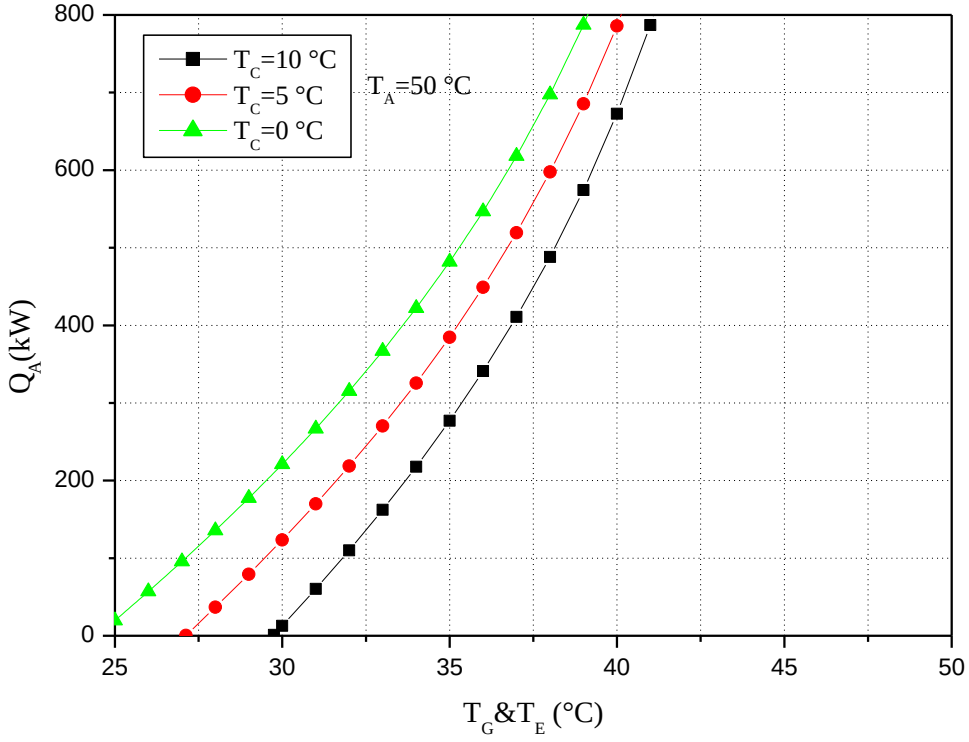

407

408 Figure 8. Effect of generator and evaporator temperature on heating capacity for SSAHT at: (a) T_A= 60
409 °C; (b) T_A= 50 °C

410

411 Figures 9(a) and 9(b) compare the circulation ratios versus the generator temperature. They show that
412 the circulation ratio for the SSAHT cycle is lower than for the SSAR cycle. This means that the circuits
413 on the solution side of the cycle must be sized in terms of the cooling loads. This lower circulation ratio
414 means that the effectiveness of the solution exchanger has less influence on the cycle COP as can be
415 seen in Fig. 10 where the cycle COP is presented for three efficiencies of the solution heat exchanger.

416

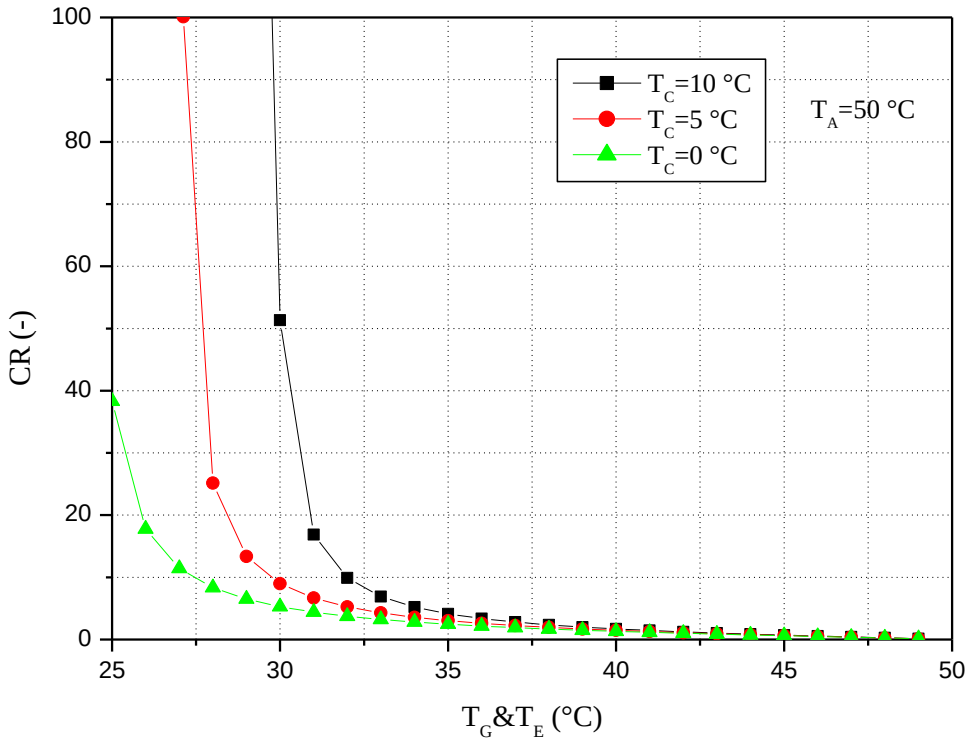

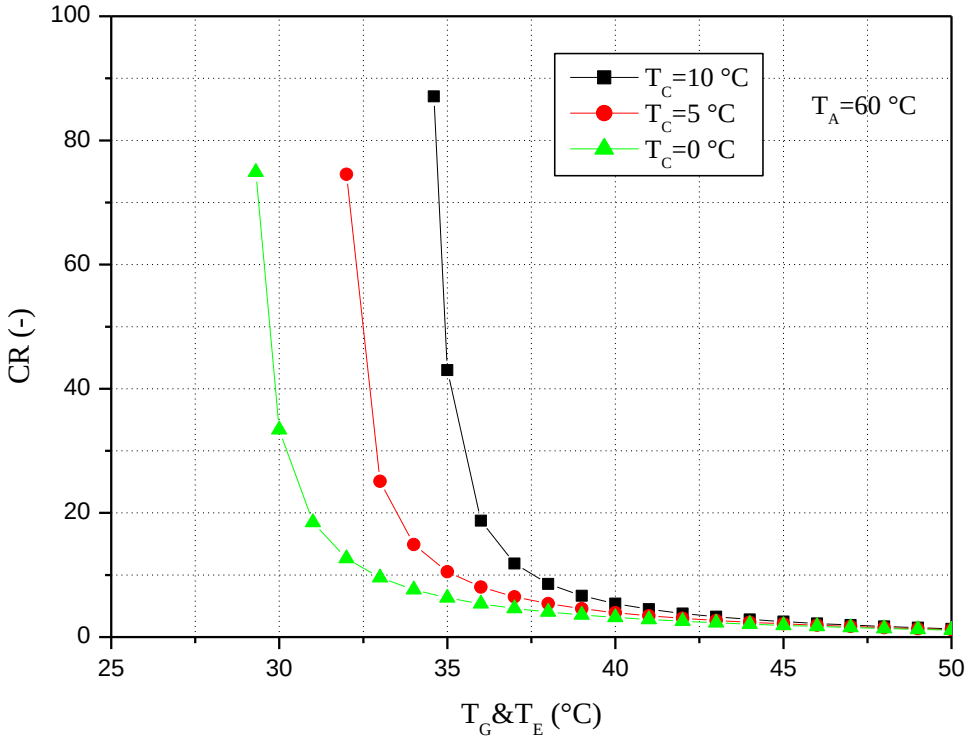

Figure 9. Effect of generator and evaporator temperature on circulation ratio for SSAHT: (a) T_A= 60 °C; (b) T_A= 50 °C

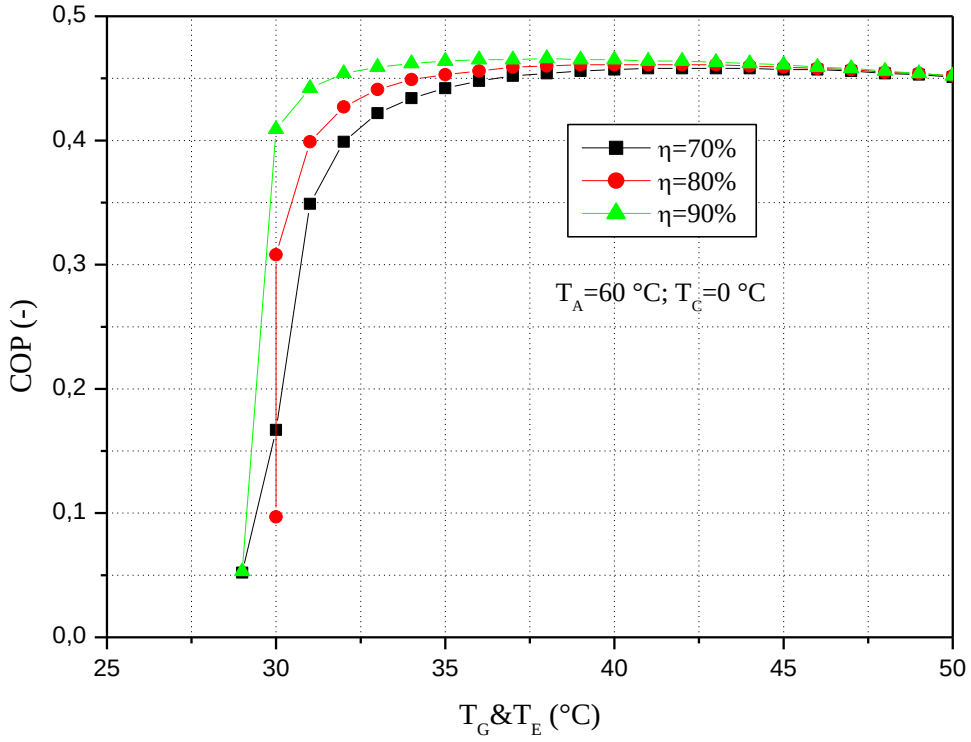

Figure 10. Effect of solution heat exchanger effectiveness on the COP of SSAHT at T_A= 60 °C

Finally, Figure 11 shows the maximum gross temperature lift (GTL) that can be reached with the SSAHT for the four T_G =T_E considered. The absorber temperatures have been obtained considering a minimum COP value of 0.44, since below this value the COP falls sharply. In each data series, the three points, from top to bottom, correspond to the three condensation temperatures (0, 5 and 10 ° C) considered in this study. The GTL increases as the temperature in the generator-evaporator increases, reaching a maximum GTL value of 34 °C for a T_G=T_E=50 °C and a condensing temperature of 0 °C. For a T_G=T_E=35 °C and a condensing temperature of 10 °C a minimum GTL value of 22 °C was obtained. On the other hand, it is observed that the maximum GTL range becomes narrower as the generator-evaporator temperature increases.

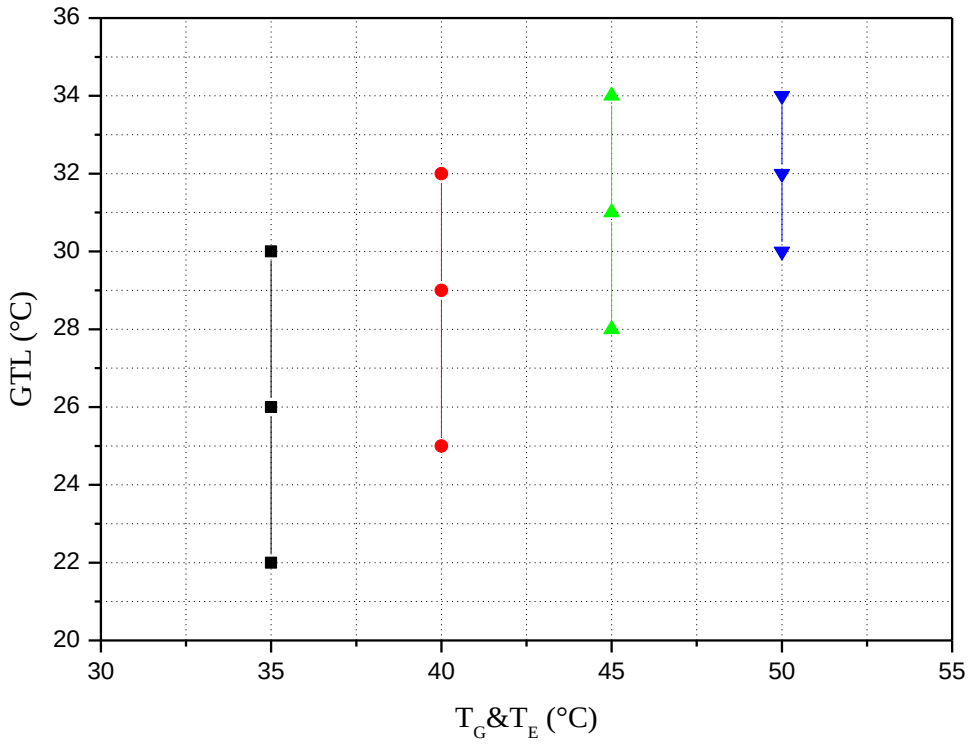

Figure 11. Variation of the maximum GTL as a function of generator-evaporator temperature

To our knowledge, only two simulation studies have been published on a SSAHT working with the NH_3-$LiNO_3$ mixture. In the first, Best et al. [17] reported data for a condensation temperature of 10 °C and a low evaporation temperature of 45 °C. However, in the generator and absorber they considered a minimum temperature of 55 and 80 °C, respectively. As a result of the higher temperature lift, a lower COP of 0.328 was obtained. The second study by Hernández-Magallanes et al. [18] focused on the energy revaluation of waste heat, but at higher heat source temperatures, since the minimum supply temperature considered was 70 °C. Also the condensation temperatures were higher since the minimum condensation temperature contemplated was 30 °C. Nonetheless, it is worth pointing out that in the stable COP range, the COP values were in the range 0.45-0.5, close to those found here.

As regards the comparison with the conventional working pair NH_3-H_2O, the experimental study presented by Garone et al. [37] considers a lower operating temperature range that is close to that of the present study. For instance, for a water inlet temperature to the condenser, generator-evaporator and absorber of 10, 60 and 70 °C, respectively, the COP value was 0.47. For a temperature lift of 10 °C, the results are similar to those obtained here. Wakim and Rivera-Tinoco [38] also studied the performance of a SSAHT with the working pair NH_3-H_2O but at a condensation temperature of 25 °C and generator-evaporator temperatures above 60 °C. Their results for COP, CR and GTL are similar to those presented here. But again, it must be considered that the absence of a rectifier with the NH_3-$LiNO_3$ mixture simplifies the structure of the cycle and the switch between the SSAR and SSAHT cycles.

6. Conclusions

A thermodynamic analysis was made of an NH_3-$LiNO_3$ reversible absorption cycle, which operates as a single-stage absorption refrigeration cycle (SSAR) in the cooling mode and as a single-stage absorption heat transformer (SSAHT) in the heating mode. The cycle is activated with solar thermal energy to meet the cooling and heating demands of a building. The components of both cycles are the same, and the only change is the flow direction inside the system.

Using a thermodynamic model, we present the effects of operation temperatures on the performance, the capacity and the circulation ratio of SSAR and SSAHT cycles. Then, combining the simulated performance with climatic conditions and available hot water temperature in winter and summer, we analyze the applicability of both cycles to provide heating and cooling demands. The most significant results are summarized below:

1. The SSAR cycle, driven with hot water temperatures that can be reached using flat collectors in summer, can provide chilled water for fan-coils or for an underfloor cooling system. A geothermal dissipation system provides COP values above 0.6 with hot water temperatures below 80 °C. A dry cooler would need heat source temperatures higher than 90 °C. The effectiveness of the solution exchanger should be as high as possible to maximize the COP of the cycle.

2. The SSAHT cycle, driven with hot water temperatures that can be reached using flat collectors in winter, can provide hot water for a conventional heating system with radiators or for an underfloor heating system. In this case, the heat dissipation would always be with a dry cooler and the activation temperature of the cycle decreases as the ambient temperature decreases. At an ambient temperature below 0 °C the cycle could be driven with hot water below 40 °C with a COP close to 0.45. The circulation ratio of the SSAHT cycle is lower than that of the SSAR cycle. Therefore, if the heating and cooling loads are similar, the components of the cycle should be sized according to the cooling load.

7. Acknowledgments

The authors would like to acknowledge financial support from the Spanish Ministry of Economy and Competitiveness RTI2018-093849-B-C33 and the Catalan Government for the quality accreditation given to their research group (2017 SGR 1409).

References

[1] Directive 2010/31/EU of the European Parlament and of the Council of 19 May 2010 on the energy performance of buildings.

[2] Henning, H-M.; Döll, J. *Solar systems for heating and cooling buildings.* Energy Procedia, 2012, vol. 30, pp. 633-653.

[3] Lazzarin, R.M., *Solar cooling: PV or thermal? A thermodymamic and economical analysis.* Internatinal Journal of Refrigeration, 2014, vol. 39, pp. 38-47.

[4] Shah, N.N.; Wilson, C.; Huang M. J.; Hewitt, N.J. *Analysis on field trial of high temperature heat pump integrated with thermal energy storage in domestic retrofit installation.* Applied Thermal Engineering, 2018, vol. 143, pp. 650-659.

[5] International Energy Agency. Solar cooling position paper. Task 38 Solar Air-Conditioning Refrigeration. Solar Heating and Cooling Program. (2011).

[6] Al-Alili, A.; Hwang, Y.; Radermacher R,. *Review of solar thermal air conditioning technologies.* International Journal of Refrigeration, 2014, vol. 39, pp. 4-22.

[7] Kim D.S.; Infante Ferreira C.A. *Solar refrigeration options – a state-of-the-art review*. International Journal of Refrigeration, 2008, vol. 31, pp. 3-15.

[8] Aliane, A.; Abboudi S.; Seladji, C.; Guendouz, B. *An illustrated review on solar absorption cooling experimental studies*. Renewable and Sustainable Energy Reviews, 2016, vol. 65, pp. 443-458.

[9] Ghafoor, A.; Munir, A. *Worldwide overview of solar thermal cooling technologies*. Renewable and Sustainable Energy Reviews, 2015, vol. 43, pp. 763-774.

[10] Siddiqui, M.U.; Said, S.A.M. *A review of solar powered absorption systems.* Renewable and Sustainable Energy Reviews, 2015, vol. 42, pp. 93-115.

[11] Bataineh, K.; Taamneh, Y. *Review and recent improvements of solar sorption cooling systems*. Energy and Buildings, 2016, vol. 128, pp. 22–37.

[12] Wu, W.; Wang, B.; You, T.; Shi, W.; Li, X. *Configurations of solar air source absorption heat pump and comparisons with conventional solar heating.* Applied Thermal Engineering, 2018, vol. 141, pp. 630-641.

[13] Li, X.; Wu, W.; Zhang, X.; Shi, W.; Wang, B. *Comparisons of different working pairs and cycles on the performance of absorption heat pump for heating and domestic hot water in cold regions.* Applied Thermal Engineering, 2012, vol. 48, pp. 349-358.

[14] Wu, W.; Zhang, X.; Li, X.; Shi, W.; Wang, B. *Energy saving potential of low temperature hot water system based on air source absorption heat pump.* Applied Thermal Engineering, 2012, vol. 48, pp. 317-334.

[15] Xu, Z.; Wang, R. *Absorption heat pump for waste heat reuse: current states and future development*. Energy 2017, vol. 11, pp. 414–436.

[16] Rivera, W.; Best, R.; Cardoso, M.J.; Romero, R.J. *A review of absorption heat transformers.* Applied Thermal Engineering, 2015, vol. 91, pp. 645-670.

[17] Best, R.; Rivera, W.; Pilatowsky I.; Holland F.A. *Thermodynamic design data for absorption heat transformers-part four. Operating on ammonia-lithium nitrate*. Heat recovery systems & CHP, 1990, vol. 10, pp. 539-548.

[18] Hernández-Magallanes,] J.A.; Rivera, W.; Coronas, A. *Comparison of single and double stage absorption and resorption heat transformers operating with the ammonia-lithium nitrate mixture.* Applied Thermal Engineering, 2017, vol. 125, pp. 53-68.

[19] Sun, D. *Comparison of the performance of NH_3-H_2O, NH_3-$LINO_3$ and NH_3-NaSCN absorption refrigeration systems*. Energy Conversion Management, 1998, vol. 31, pp. 357-368

[20] Cerezo, J.; Romero, R. J.; Ibarra, J.; Rodríguez, A.; Montero, G.; Acuña, A. *Dynamic Simulation of an Absorption Cooling System with Different Working Mixtures*. Energies, 2018, vol. 11, pp. 259.

[21] De Vega, M.; Venegas, M.; García-Hernando, N. *Modeling and performance analysis of an absorption chiller with a microchannel membrane-based absorber using LiBr-H_2O, LiCl-H_2O, and $LiNO_3$-NH_3*. International Journal of Energy Research, 2018, vol. 42, pp. 3544–3558.

[22] Antonopoulos, K.A.; Rogdakis, E.D. *Performance of solar-driven ammonia-lithium nitrate and ammonia—sodium thiocyanate absorption systems operating as coolers or heat pumps in Athens*. Applied Thermal Engineering, 1996, vol. 16, pp. 127-147.

[23] Abdulateef, J.M.; Sopian, K.; Alghoul, M.A. Optimum design for solar absorption refrigeration systems and comparison of the performances using ammonia-water, ammonia-lithium nitrate and ammonia-sodium thiocyanate solutions. International Journal of Mechanical and Materials Engineering, 2008, vol. 3, pp. 17-24.
[24] Hernandez-Magallanes, J.A.; Domínguez-Inzunza, L.A.; Gutierrez-Urueta, G.; Soto, P.; Jimenez, C.; Rivera, W. *Experimental assessment of an absorption cooling system operating with the ammonia/lithium nitrate mixture*. Energy, 2014, vol. 78, pp. 685-692.
[25] Zamora, M.; Bourouis, M.; Coronas, A.; Vallès, M. *Pre-industrial development and experimental characterization of new air-cooled and watercooled ammonia/lithium nitrate absorption chillers*. International Journal of Refrigeration, 2014, vol. 45, pp. 189-197.
[26] Zamora, M.; Bourouis, M.; Coronas, A.; Vallès, M. *Part-load characteristics of a new ammonia/lithium nitrate absorption chiller.* International Journal of Refrigeration, 2014, vol. 56, pp. 43-51.
[27] Ibarra-Bahena, J.; Romero, R. J. *Performance of Different Experimental Absorber Designs in Absorption Heat Pump Cycle Technologies: A Review.* Energies, 2014, vol. 7, pp. 751-766.
[28] Oronel, C.; Amaris, C.; Bourouis, M.; Vallès, M. *Heat and mass transfer in a bubble plate absorber with $NH_3/LiNO_3$ and $NH_3/(LiNO_3 + H_2O)$ mixtures*. International Journal of Thermal Sciences, 2013, vol. 63, pp. 105-114.
[29] Táboas, F.; Bourouis, M.; Vallès, M. *Boiling heat transfer and pressure drop of $NH_3/LiNO_3$ and $NH_3/(LiNO_3 + H_2O)$ in plate heat exchangers*. International Journal of Thermal Sciences, 2016, vol. 105, pp. 182-194.
[30] Panchal, C. B.; Rabas, T.J. *Thermal performance of advanced heat exchangers for ammonia refrigeration systems*. Heat transfer engineering, 1993, vol. 14, pp. 42-57.
[31] Khan, T.S.; Hhan, M.S.; Chyu, M-C.; Ayub, Z. H. *Experimental investigation of evaporation heat transfer and pressure drop of ammonia in a 60° chevron plate heat exchanger.* International Journal of Refrigeration, 2012, vol. 35, pp. 336-348.
[32] Tillner-Roth, R.; Harms-Watzenberg, F.; Baehr H.D. *Eine neue Fundamentalgleichung für Ammoniak*. DKV-Tagunsbericht, 1993, vol. 20, pp. 357-368.
[33] Salavera, D.; Coronas, A. *Property modeling of the ammonia+lithium nitrate from new experimental data for absorption refrigeration applications*. International Conference on Cryogenics and Refrigeration, 2018, Shanghay.
[34] Táboas, F.; Bourouis, M.; Vallès, M. *Analysis of ammonia/water and ammonia/salt mixture absorption cycles for refrigeration purposes in fishing ships.* Applied Thermal Engineering, 2014, vol. 66, pp. 603-611.
[35] Ayala, R.; Heard, C.L.; Holland, F.A. *Ammonia/lithium nitrate absorption/compression cycle. Part I. Simulation.* Applied Thermal Engineering, 1997, vol. 17, pp. 223-233.
[36] Dominguez-Inzunza, L.A.; Hernández-Magallanes, J.A.; Sandoval-Reyes, M.; Rivera W. *Comparison of the performance of single-effect, half-effect, double-effect in series and inverse and triple-effect absorption cooling systems operating with the NH3eLiNO3 mixture.* Applied Thermal Engineering, 2014, vol. 66, pp. 612-620.
[37] Garone, S.; Toppi, T.; Gerra, M.; Motta, M. *A water-ammonia heat transformer to upgrade low-temperature waste heat.* Applied Thermal Engineering, 2017, vol. 127, pp. 748-757.
[38] Wakim, M.; Rivera-Tinoco, R. *Absorption heat transformers: Sensitivity study to answer existing discrepancies.* Renewable energy, 2019, vol. 130, pp. 881-890.

List of figures

List of tables